Determination of cross-tissue and tissue-specific aging changes in murine proteomes

Gregory R. Keele[1], Ji-Gang Zhang[1], John Szpyt[2], Ron Korstanje[1], Steven P. Gygi[2], Gary A. Churchill[1#], Devin K. Schweppe[3#]

[1]The Jackson Laboratory, Bar Harbor, ME 04609, USA

[2]Department of Cell Biology, Harvard Medical School, Boston, MA 02115, USA

[3]Department of Genome Sciences, University of Washington, Seattle, WA 98105, USA

#Corresponding authors

Corresponding author: gary.churchill@jax.org, dkschwep@uw.edu

ABSTRACT

Maintenance of protein homeostasis degrades with age, contributing to aging-related decline and disease. Previous studies have primarily surveyed transcriptional changes with age. We sought to define the effects of age directly at the protein level. We performed discovery-based proteomics in 10 tissues from 20 C57BL/6J mice, representing both sexes at adult and late midlife ages (8 and 18 months). We find that sex differences in protein abundance align closely with previously collected transcriptomics data. However, aging changes are more prevalent in proteins and often have no corresponding transcriptional change. We observed increases in immune protein abundance across all tissues, consistent with immune infiltration with age. We also observed tissue-specific aging changes, including altered endoplasmic reticulum and protein trafficking protein abundances in the spleen, and altered stoichiometry in protein complexes related to proteostasis, such as the chaperonin-containing T-complex. This study provides a foundation for understanding systemic aging at the protein level.

23 **INTRODUCTION**

24 Aging results in a progressive decline in physiological function that increases risk of disease and
25 ultimately death[1]. Gene expression studies have revealed age-related changes in transcripts that are
26 shared across tissues, and others that are tissue-specific[2–4], as well as transcripts that contrast healthy
27 and diseased aging in humans[5]. However, these studies are unable to directly ascertain age-related
28 changes in proteins. Untargeted, quantitative proteomics studies can reveal how proteins change with
29 age, which can confirm findings from gene expression, but more importantly, they can identify
30 molecular aging signatures that occur independently of gene expression changes.

31 We have previously investigated the effects of age and sex on gene expression and protein
32 abundance in kidneys[6] and hearts[7] from genetically diverse mice. We found that differences in protein
33 abundance between males and females in the kidney were largely mediated through their transcripts. In
34 contrast, differences in protein abundance across ages were largely independent of their transcripts. A
35 similar dynamic between sex and age differences was observed in heart, although fewer sex differences
36 were present. From these studies, we concluded that many age-related changes in protein abundance
37 are not due to corresponding changes in gene expression and that transcriptomics provides an
38 incomplete picture of aging in kidney and heart. Multiple mechanisms could result in decoupling
39 proteins from their transcripts with age, including reduced proteasome activity[8] and reduced ribosome
40 occupancy[9] with age.

41 A key question is whether this discordance between protein abundance and gene expression
42 occurs for most tissues. Furthermore, we are interested in which age-related changes are shared across
43 tissues and which are unique. Comparing the kidney and heart revealed common signatures of
44 increased immune cell infiltration in both tissues for proteins and transcripts. We also observed tissue-
45 specific changes, particularly among proteins. Changes in the kidney proteome correspond to functions

46 specific to the substructures and cell subtypes of the nephron, including the podocytes and proximal
47 tubule cells. In the heart, we observed age-related changes in fatty acid metabolism and autophagy.
48 These tissue-specific changes relate to the unique biological functions and stressors of these tissues
49 during aging.

50 To address these questions, we performed a survey of protein abundance across ten tissues
51 (kidney, liver, fat, spleen, lung, heart, skeletal muscle, striatum, cerebellum, and hippocampus) collected
52 from female and male C57BL/6J mice at 8 and 18 months of age. We performed multiplexed,
53 quantitative mass spectrometry on bulk tissue samples and analyzed differences in protein abundance
54 between age and sex, as well as sex-specific changes with age. We compared age and sex differences for
55 proteins in our study to transcript changes in corresponding tissues that were reported by Schaum *et al*
56 2020[2]. We used enrichment analyses to assess how aging affects biological processes, as reflected by
57 coordinated changes in proteins across and within tissues. Finally, we characterized aging-related
58 changes to protein complexes, in terms of overall and relative abundances of member proteins. Our
59 findings confirm the discordance between age-related changes in proteins and gene expression across
60 multiple tissues. Our data provide a broad survey of shared and tissue-specific changes in proteins in the
61 aging cell, many of which occur independently of transcription.
62

63 **RESULTS**

64 We quantitatively profiled protein abundance across 10 tissues (Table S1) representing a range of organ
65 systems (kidney, liver, fat, spleen, lung, heart, skeletal muscle, striatum, cerebellum, and hippocampus)
66 from 20 C57BL/6J (B6) mice using tandem mass tags (TMT) and real-time search (RTS) mass
67 spectrometry[10]. Animals represented an equal balance across males, females, and two age groups (8 and
68 18 months), resulting in five animals per sex-by-age group. Outlying samples for each tissue were
69 identified using principal component analysis (PCA), resulting in the removal of one sample from liver,

70 fat, spleen, lung, and skeletal muscle, and two samples from striatum (Methods). Cumulatively, we
71 detected 11,853 proteins across the 10 tissues, and after filtering out proteins identified in only a single
72 batch, 10,250 were used in further quantitative analysis. Spleen had the highest number of analyzed
73 proteins (6,556) and skeletal muscle had the fewest (2,353) (Upset plot[11] in Figure 1C). Many proteins
74 were detected across multiple tissues. We observed 676 different protein-to-tissue overlap sets, with
75 detection in all tissues being the most common (1,229) followed by proteins detected in only spleen
76 (1,003) and then only the three brain tissues (425) (Figure 1D).

77 To assess how different technical features of the experiment contributed to variation in the
78 abundance of individual proteins, we jointly modeled data across tissues by fitting random effects
79 models (Methods) for each of the 1,229 proteins measured in all 10 tissues (Table S2). As expected, the
80 primary source of variation is batch, which is confounded with tissue and represents 20 separate runs of
81 the mass spectrometer (Figure S1A). We also identified 13 proteins that had abundance patterns that
82 were highly specific to an individual mouse across the 10 tissues, including IGHG2C and four other
83 immunoglobulins (Figure S1B-D). Using gene set enrichment analysis[12] (Methods), the 13 proteins
84 (compared to the overall set of 1,229 proteins observed in all tissues) were enriched for gene ontology
85 (GO) terms related to adaptive immune response.

86 **Effects of age and sex on the abundance of individual proteins**

87 Protein abundance can vary between the sexes[13–15] and with age[6,7,16]. For each tissue, we characterized
88 age and sex effects (Table S3) and declared differences to be significant based on false discovery rate
89 (FDR) < 0.1 (Figures 2 and S2, respectively; Methods). The number of proteins with age effects varied
90 greatly across the tissues, ranging from lung with the most (866) to striatum with none meeting
91 statistical significance (partially due to loss of power from the removal of two animals). The number of
92 proteins with sex effects also varied across the tissues, from kidney with 2,175 to the three brain tissues

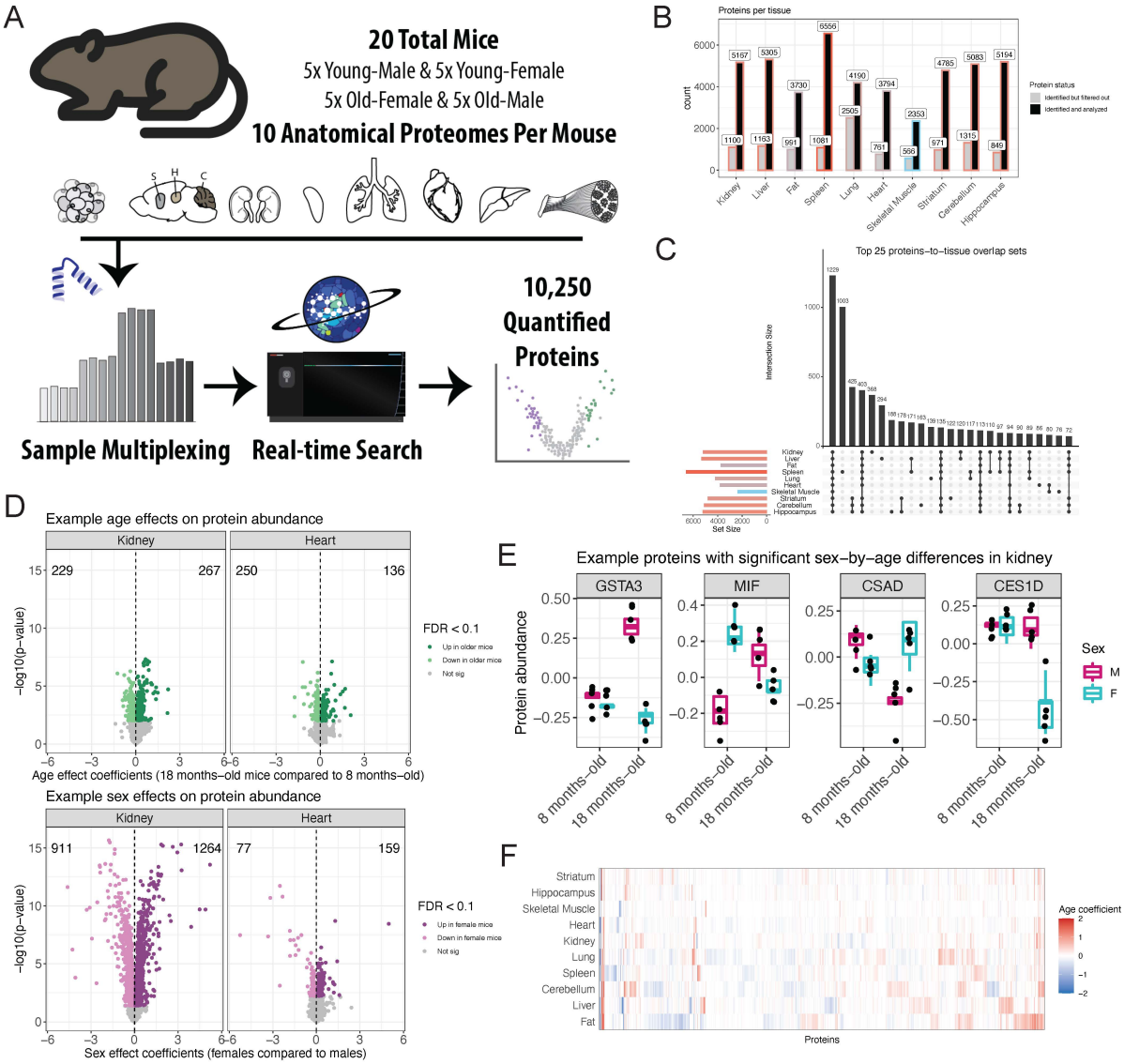

Figure 1. Quantitative proteomics study on the effects of age and sex on protein abundance across 10 tissues from B6 mice.

(A) Using sample multiplexing, 10 anatomical proteomes (adipose tissue, striatum, hippocampus, cerebellum, kidney, spleen, lung, heart, liver, skeletal muscle) were profiled across age and sex matched mice (n=20).
(B) The number of proteins analyzed and filtered out due to detection in only a single batch across the 10 tissues.
(C) The top 25 intersections of proteins and the tissues in which they were detected and analyzed.
(D) Age (top) and sex (bottom) differences for protein abundance from kidney (left) and heart (right) tissues, depicted as volcano plots. Differences in protein abundance are summarized as regression coefficients (x-axis) and corresponding -$\log_{10}$(*p*-value) (y-axis). Points are colored based on statistical significance (FDR < 0.1) and direction of effect. Counts of proteins with significantly higher abundance in older mice and younger mice are included. Dashed vertical lines at 0 included for reference.
(E) Examples of proteins in kidney tissue with significant sex-by-age differences (FDR < 0.1).
(F) Age differences detected across the 10 tissues (FDR < 0.1), represented as a heatmap. Differences are summarized as regression coefficients.

108 with 10 or fewer. We also identified proteins for which sex differences in abundance depended on age
109 by testing for sex-by-age interaction effects (Methods), detecting 21 in kidney, 6 in liver, 5 in fat, and 11
110 in skeletal muscle (FDR < 0.1) (Figure S3). The skeletal muscle proteins, for which males had distinctly
111 higher abundance than females in older mice, were associated with the endoplasmic reticulum lumen.
112 Comparison of sex and age effects across the tissues revealed generally more differences between sexes
113 than between ages, most notably in kidney, liver, fat, and spleen. However, proteins with significant age
114 effects outnumbered those with sex effects in lung, heart, and cerebellum (Figure S4). The three brain
115 tissues were distinctly buffered from differences based on age and sex. In total, 2,356 proteins had a
116 significant age effect in at least one tissue, 5,125 had a sex effect, and 43 had a sex-by-age interaction
117 effect (FDR < 0.1).

118 We jointly modeled data across multiple tissues for individual proteins (Methods) to test
119 whether the age or sex effects on proteins were consistent across tissues or unique to specific tissues
120 (Table S4), declaring significance based on FDR < 0.1. From the 7,745 proteins detected in more than
121 one tissue, 643 had consistent age differences across the tissues in which they were quantified. For
122 example, IKGC is an immunoglobulin that has increased abundance in older mice for all tissues (cross-
123 tissue age p = 1.1e-6; Figure 2B). We detected 1,028 proteins with age effects that differed between
124 tissues, representing proteins that had age differences in only some of the tissue or even age effects
125 with differing directions, such as BCAT1 (age-by-tissue p = 1.8e-10), CES1D (age-by-tissue p = 1.1e-10),
126 FBLN1 (age-by-tissue p = 2.1e-8), and STAB1 (age-by-tissue p = 2.6e-8) (Figure 2C). These age-related
127 differences may contribute to aging decline. For example in kidney, there was reduced abundance of
128 BCAT1, which promotes mitochondrial biogenesis and ATP production and has been shown to promote
129 breast cancer formation when knocked down[17], and REN1, which has been shown to play a role in
130 modulating vascular tone and tubular function in the kidney[18]. For sex effects, we detected 1,006

proteins with consistent differences between sexes across tissues and 2,565 proteins with tissue-specificity.

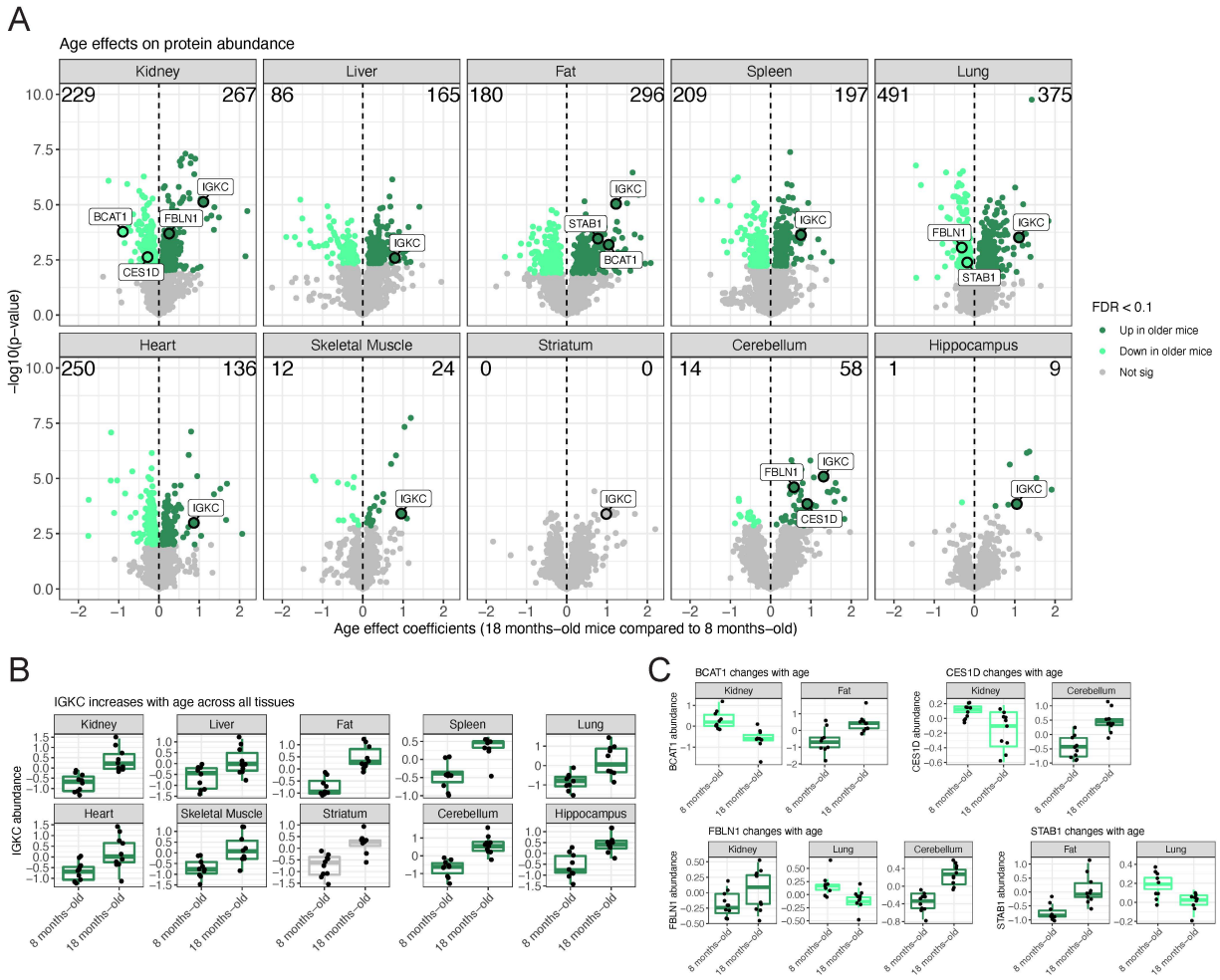

Figure 2. Proteins with age-related differences in abundance, across 10 tissues.
(A) Proteins with age differences in abundance, represented as volcano plots. Differences in protein abundance are summarized as regression coefficients (x-axis) and corresponding -$\log_{10}$(p-value) (y-axis). Points are colored based on statistical significance (FDR < 0.1) and direction of effect. Counts of proteins with significantly higher abundance in older mice and younger mice are included. Dashed vertical lines at 0 included for reference. Proteins with sex differences in abundance are shown in Figure S2.
(B) The immunoglobulin IGKC has consistent increased abundance in older mice across all 10 tissues.
(C) Proteins with significant age differences that vary between tissues: BCAT1, CES1D, FBLN1, and STAB1.

Age effects are less consistent between proteins and transcripts than sex effects

144 To compare sex and age effects on proteins to corresponding effects on transcripts, we obtained data
145 from Schaum *et al* 2020[2], in which bulk RNA sequencing was performed across 17 tissues at 10 ages,
146 ranging from 1 to 27 months. Each age group consisted of 4 to 6 C57BL/6JN mice. Overlapping tissues
147 between studies include kidney, liver, and heart. We selected the transcriptomics data from the 9 and
148 18 months age groups, which are closest to 8 and 18 months in the proteomics data, and characterized
149 the sex and age effects on transcripts (Methods).

150 The sex effects on proteins and transcripts are more consistent than age effects, most notably in
151 kidney and liver (Figures 3A-C). We observed a similar dynamic in kidney tissue as was seen in
152 genetically diverse mice[6]. The similarity in sex effects is strong despite being evaluated in mice from
153 distinct (but related) strains, raised at different sites, and as part of different experiments. Genes with
154 consistent age effects on transcripts and proteins in kidney include *Keg1* and *Vcam1* (Figures 3D-E).
155 VCAM1 is an immunoglobulin that facilitates interactions between vascular and immune cells and its
156 increase with age has been associated with age-related disease in humans[19–21]. We observed increases
157 in VCAM1 abundance with age across multiple tissues (kidney, liver, fat, and cerebellum), which resulted
158 in a significant cross-tissue age effect (cross-tissue age p = 1.59e-7).

159 Despite heart tissue having far fewer significant sex effects than kidney or liver, consistent with
160 our previous work[7], they are still more consistent between proteins and transcripts than age effects.
161 Notable genes with consistent sex effects on transcripts and proteins are *Ddx37* and *Eif2s3x* which are
162 encoded on the Y and X chromosomes, respectively. These findings validate the quality of the protein
163 data by demonstrating the consistency of sex effects with transcript data. They also highlight the
164 importance of assessing aging-related changes among proteins, many of which are not observed at the
165 transcript level.

166 **Immune system change is a signature of aging across all 10 tissues**

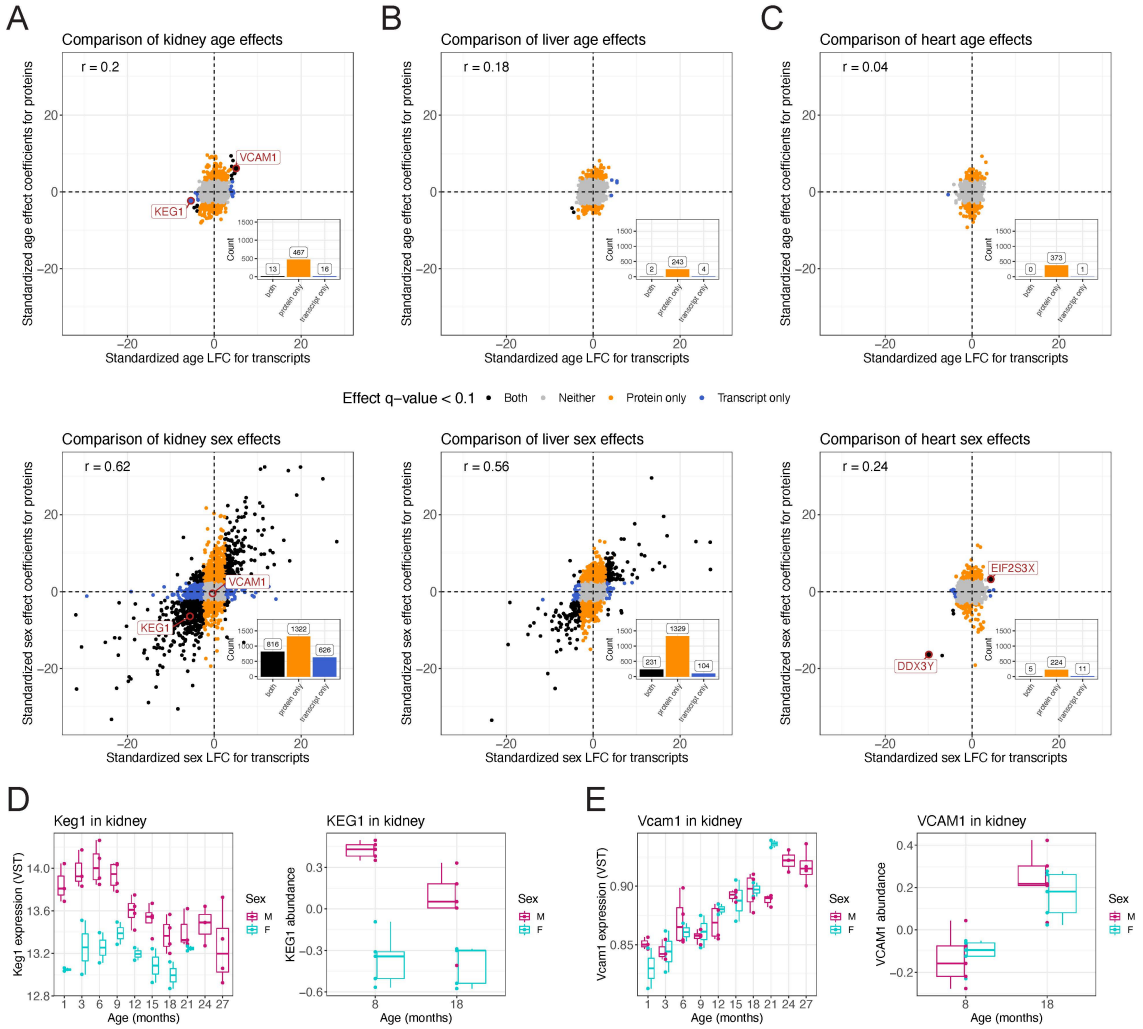

Figure 3. Age-related differences are less shared between protein and transcripts than sex-related differences. Comparisons of age- (top) and sex-related (bottom) differences in proteins to transcripts in (A) kidney, (B) liver, and (C) heart. Points are colored based on statistical significance (FDR < 0.1) in proteins and transcripts. Dashed vertical and horizontal lines at 0 included for reference. Counts of genes with significant differences included as bar plots in the bottom right quadrant.
(D) *Keg1* expression had significant age and sex differences (left), whereas its protein had a matching sex effect (right). The age effect did not meet significance at FDR < 0.1, but the direction is consistent with transcripts.
(E) *Vcam1* significantly increase with age in terms of both transcripts (left) and proteins (right).

We clustered the 2,356 proteins that had significant age effects in at least one tissue after setting effects to zero in tissues in which proteins were not observed. Looking broadly across the clustered age effects reveals consistent immune-related differences between age groups across all 10 tissues (Figure 4A). Components of the innate immune system, most notably C8A and C8B, were less abundant in all tissues of older mice. Immunoglobins and other proteins related to humoral immunity were distinctly more

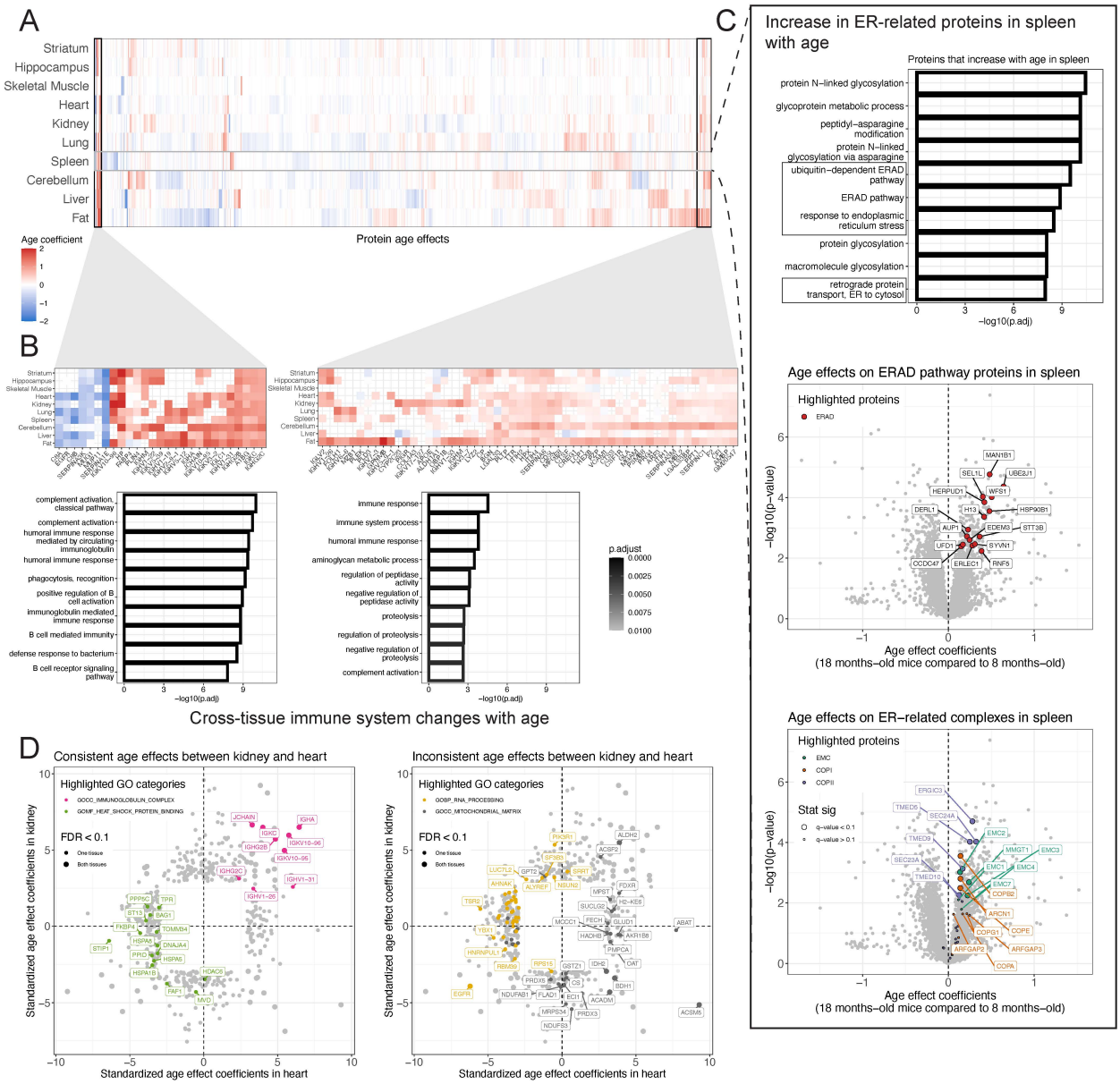

Figure 4. Cross-tissue and tissue-unique patterns of aging.
(A) Age-related differences detected across the 10 tissues (FDR < 0.1), represented as a heatmap. Differences are summarized as regression coefficients. Hierarchical clustering of the proteins (columns) reveals sets of proteins with age difference patterns across tissues and unique to specific tissues.
(B) Proteins with age differences that are shared across tissues are enriched for immune-related GO categories. Additional tissue-unique patterns are highlighted in Figure S5.
(C) The proteins with age differences in a specific tissue can be enriched in GO categories, with spleen highlighted here for proteins with higher abundance in older mice. Abundance differences with age for proteins analyzed in spleen, represented as volcano plots. Differences in protein abundance are summarized as regression coefficients (x-axis) and corresponding -$\log_{10}$(p-value) (y-axis). The ERAD pathway, EMC, COPI, and COPII proteins are highlighted. Highlighted proteins with significant differences (FDR < 0.1) have larger point size. Proteins with age p < 0.05 were labeled.

195 (D) Comparison of age differences between kidney and heart with highlighted GO categories that are consistent
196 (left) and inconsistent (right) between the tissues. Proteins with a significant age difference (FDR < 0.1) in kidney or
197 heart are shown. Proteins with significant differences (FDR < 0.1) in both tissues have a larger point size.

198

199 abundant in older mice. Proteins involved in proteolysis, including immunoproteasomes like PSMB8,
200 were also more abundant in older mice to varying degrees across the 10 tissues.

201 The consistency of age effects across tissues for immune-related proteins is striking, as
202 highlighted by the adaptive immune response GO set (GO:0002250) (Figure 5A). Even tissues with few
203 statistically significant age effects, most notably striatum with none, show differences in the same
204 direction, such as increased abundance of immunoglobins in older mice. We note that the abundance of
205 the immunoproteasomes (PSMB8, PSMB9, and PSMB10) is higher in older mice for the tissues with the
206 most pronounced age-related increases in immunoglobins, fat and cerebellum (Figures 5B-C). The
207 immunoproteasomes are inducible components that replace the constitutive components (PSMB5,
208 PSMB6, and PSMB7) in the 20S catalytic core of the proteasome[22]. The immunoproteasome is more
209 efficient at degrading ubiquitin-labeled proteins as antigens for presentation on MHC class I molecules, a
210 key process in distinguishing between self and non-self in adaptive immunity[23]. The immunoproteasome
211 is not a perfect marker of immune cells however, as it is also expressed by non-immune cells during
212 inflammation[24].

213 The co-regulation of the overall proteosome complex, encompassing the 20S catalytic core, its
214 19S regulator, and the 11S regulator, is multifaceted. We have previously shown that abundance of
215 individual components and sub-complexes of the proteasome are influenced by genetic variation[14] and
216 age[7] in genetically diverse mouse populations. In this B6 sample population where genetic variation has
217 been fixed (excluding spontaneous mutations specific to individuals), the sub-complex structure of the
218 proteasome, most notably the 20S catalytic core and 19S regulator, is reflected in the pairwise
219 correlations between complex members. The individual sub-complexes become more tightly correlated

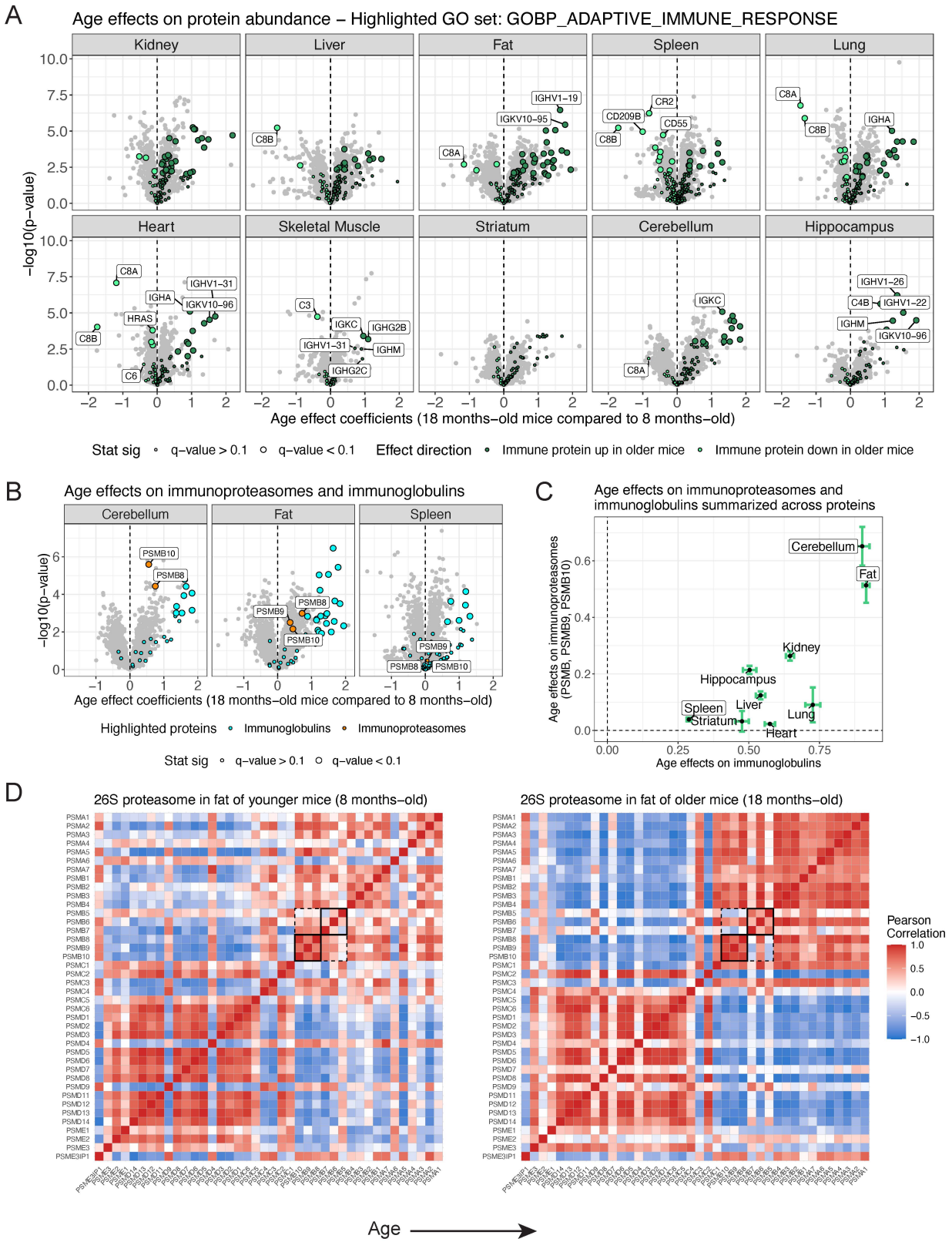

Figure 5. Increased immunoglobulin abundance is a signature of aging detected in all 10 tissues.

222 (A) Proteins with age differences in abundance, represented as volcano plots. Differences in protein abundance are
223 summarized as regression coefficients (x-axis) and corresponding -$\log_{10}$(*p*-value) (y-axis). Points are colored based
224 on being a member of the adaptive immune response GO category and direction of effect. Highlighted proteins
225 with significant differences (FDR < 0.1) have larger point size. Dashed vertical lines at 0 included for reference.
226 (B) Volcano plots for cerebellum, fat, and spleen, with immunoglobins and immunoproteasomes (PSMB8, PSMB9,
227 and PSMB10) highlighted.
228 (C) Age differences summarized across the immunoproteasomes (y-axis) and immunoglobins (x-axis) for all 10
229 tissues. Points represent mean differences and bars represent standard errors. Horizontal and vertical dashed lines
230 at 0 included for reference.
231 (D) Pearson correlations from the proteasome in younger (top) and older (bottom) mouse fat. Rows and columns
232 are ordered to reflect key sub-complexes of the proteasome, which are labeled. The immunoproteasomes and
233 their matching constitutive analogs are highlighted with black square.

234

235 within themselves (and anti-correlated with each other) in the older mice in fat tissue (Figure 5D). The
236 correlation among the immunoproteasome components (and anti-correlation with their constitutive
237 analogs) becomes more pronounced in the older mice, likely due to increased levels of
238 immunoproteasome from immune cells.

239 **Tissue-specific signatures of aging**

240 Age effects also reveal unique patterns specific to tissues (Tables S5-6). Spleen exhibits unique increases
241 in abundance for proteins related to the endoplasmic reticulum (ER), such as the ER-associated
242 degradation (ERAD) pathway, ER membrane complex (EMC), and the COPI and COPII complexes (Figure
243 4C), suggesting potential changes to protein quality control[25] in the spleen. The EMC enables the
244 biogenesis of multipass transmembrane proteins and has been associated with pleiotropic phenotypes
245 across organisms[26,27]. COPI and COPII are involved in trafficking proteins between the ER and Golgi[28]. In
246 addition to the immune signatures observed across all 10 tissues, we saw tissue-specific immune
247 patterns, such as decreased abundance for proteins involved in leukocyte and lymphocyte activation in
248 the spleens of older mice (Figure S5B) and increased abundance for proteins involved in a broad range
249 of immune system-related GO categories in the fat of older mice (Figure S5C). We observed decreased
250 abundance in older mice for proteins related to the mitochondrial chain complex I and the oxidation-
251 reduction process (Figure S5A) and increased abundance in older mice for proteins related to multiple

252 metabolic processes (Figure S5D). Comparison of gene set enrichment results between tissues can
253 highlight shared or distinct aging processes. For example, we compared kidney and heart, which
254 revealed consistent GO categories like immunoglobulins (increasing with age) and heat shock proteins
255 (decreasing with age) and inconsistent GO categories like the mitochondrial matrix and RNA processing
256 (Figure 4D).

257 **Age and sex influence the abundance and stoichiometric balance of protein complexes**

258 Individual members of protein complexes are often co-regulated to maintain stoichiometric balance of
259 components[29–33]. Biological factors can affect this balance, including genetics, sex, and age[7,13–15]. More
260 than one factor can influence a complex (or its sub-complexes or individual components), as
261 demonstrated by the effects of both genetic variation and age on the proteasome[7,14]. To measure a
262 protein complex's co-abundance, referred to here as cohesiveness, for each of 228 annotated protein
263 complexes[34,35] across the 10 tissues, we summarized across the median pairwise correlations of complex
264 members (Table S7; Methods). We note that the cohesiveness of a complex could reflect its
265 stoichiometric balance as well as cell type heterogeneity. We observed some conservation of protein
266 complex cohesiveness between tissues, most notably among the three brain tissues ($r > 0.68$, $p < 2.2e-$
267 16; Figure S6).

268 We tested whether age or sex had consistent effects on abundance across the members of a
269 protein complex (Table S7; Methods), as would be expected if the entire protein complex is changing
270 with age or sex. Examples include the previously mentioned COPI and COPII complexes in the spleen
271 (Figure 4C). The number of protein complexes with a multi-protein age effect varied across the tissues,
272 ranging from lung with 29 to skeletal muscle and hippocampus with none at FDR < 0.1 (Figure S7A).
273 More complexes had consistent sex effects across proteins, ranging from spleen with 76 to striatum and
274 cerebellum with none at FDR < 0.1 (Figure S7B).

275 Changes due to age or sex on protein complexes may be more subtle than a change in mean
276 abundance across complex members. Cohesiveness of a protein complex can vary with age or sex. We
277 first calculated the pairwise correlations among protein complex members for each age group and then
278 looked for changes in overall correlation patterns with a paired *t*-test (Table S7; Methods). The same
279 approach was used for sex. We used a stricter threshold of significance (FDR < 0.01) in order to focus on
280 only the most significant effects. The association of age with cohesiveness of complexes varied across
281 the tissues, ranging from 35 complexes in spleen to 3 in skeletal muscle at FDR < 0.01 (Figure S8A). For
282 sex, spleen had the largest number of complexes with changes in cohesiveness (26), and fat,
283 hippocampus, and striatum had the fewest with 6 each, all at FDR < 0.01 (Figure S8B). Ribosomes have
284 been shown to lose stoichiometric balance with age in the brains of killifish[8], and we see similar signals
285 across many of our tissues (Figure S8A), indicating that this previous finding generalizes across tissues
286 and species.

287 For each complex, we counted the number of tissues for which a significant age and sex effect
288 on abundance or cohesiveness were detected (Figure S9). The co-distribution of age and sex effects
289 differed between effects on abundance and effects on cohesiveness. Effects on abundance were more
290 likely to be detected in smaller subsets of tissues, whereas effects on cohesiveness represent a distinct
291 minority of complexes with both age and sex effects on cohesiveness across many tissues, such as the
292 chaperonin-containing T-complex (CCT-complex) and cytoplasmic ribosomal large subunit (CRLS).

293 **CCT-complex is more cohesive in older B6 mouse cerebellum**

294 The CCT-complex, also known as the tailless complex polypeptide 1 ring complex (TRiC), is required for
295 folding proteins such as acting and tubulin. The CCT-complex was significantly more cohesive in older
296 mouse cerebellum than in younger (p = 2.0e-8; Figure 6). This signal is due to CCT6A, CCT2, CCT5, and to
297 a lesser extent CCT3, being anti-correlated with other complex members in younger mice but more

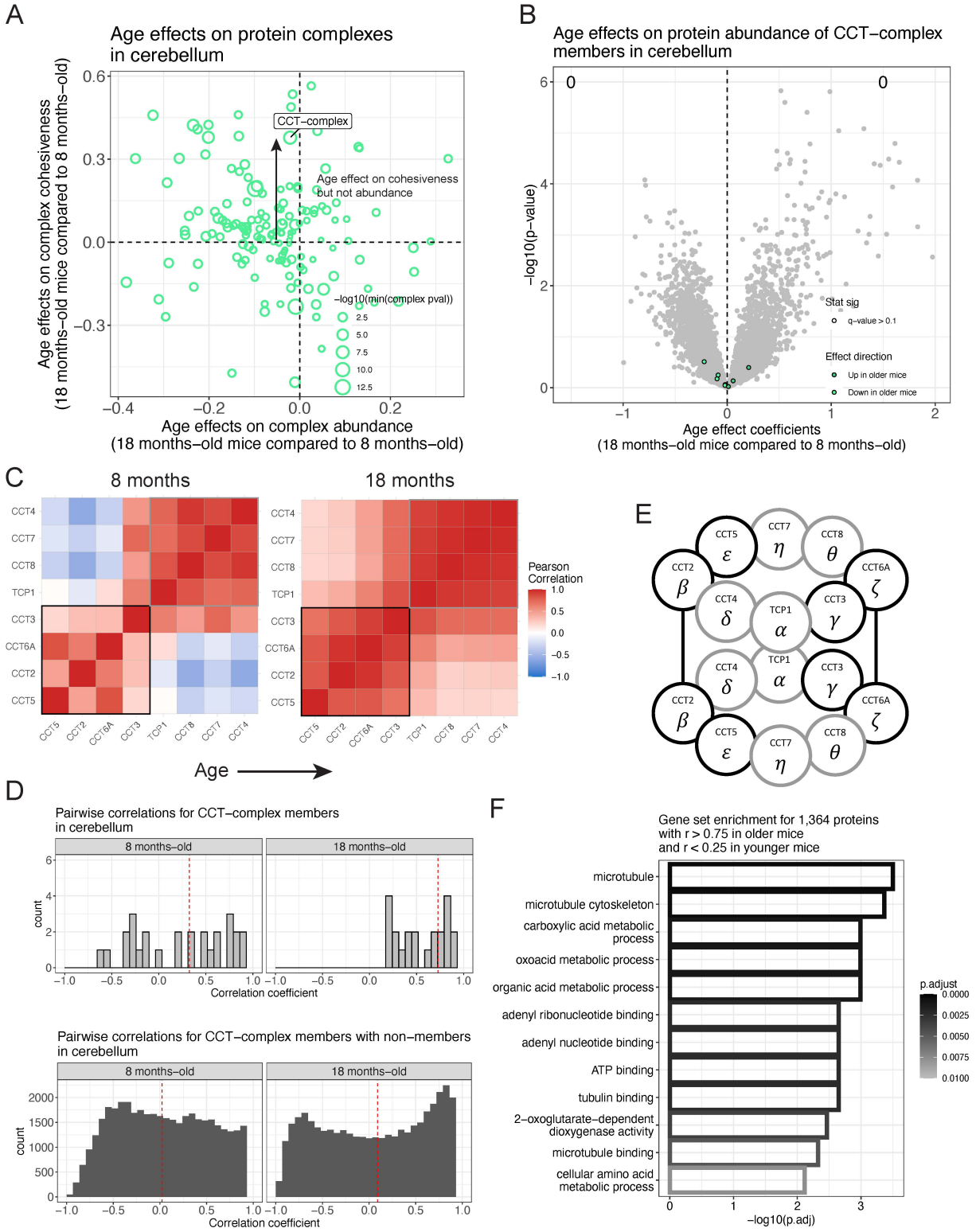

Figure 6. CCT-complex is more stoichiometrically balanced in older mouse cerebellum.
(A) Comparison of age-related differences in complex-wide correlation (y-axis) to complex-wide abundance (x-axis) in cerebellum. Point size corresponds to the minimum p-value from the complex-wide correlation and complex-wide abundance tests on the -log10 scale. CCT-complex is highlighted.

303 (B) Volcano plot for age differences in individual protein abundance for cerebellum with CCT-complex members
304 highlighted with color based on direction of effect. Counts of proteins with significantly higher abundance in older
305 mice and younger mice are included (FDR < 0.1).
306 (C) Pearson correlations from the CCT-complex in younger (left) and older (right) mouse cerebellum. Black and gray
307 squares highlight patterns in the correlation matrix that mirror the structure of the CCT-complex.
308 (D) Histograms of pairwise correlation coefficients between CCT-complex members with each other (top) and
309 other proteins (bottom). Vertical red dashed lines represent median correlations.
310 (E) The CCT-complex is composed of two identical octomeric rings. The CCT2 (β) and CCT6A (ζ) from each ring are
311 in physical with their twin. Outline of proteins matches correlation structure previously highlighted.
312 (F) GO categories enriched in proteins that are more correlated with CCT-complex members in older mouse
313 cerebellum than younger. The microtubule GO category (GO:0005874) is explored further in Figure S10.

314

315 correlated in older mice (Figure 6B). The significance of the change of individual pairwise correlations
316 were determined using permutations (Methods). The pattern of correlations reflects the physical
317 structure of the CCT-complex, which is composed of two octameric rings made from eight proteins
318 (TCP1, CCT2, CCT3, CCT4, CCT5, CCT6A, CCT7, and CCT8)[36,37] (Figure 6E). Notably, the CCT6A and CCT2
319 components from the upper and lower rings are in physical contact with their matching protein. CCT5
320 and CCT3 are immediately adjacent to CC2 and CCT6A, respectively, in both rings. We have previously
321 shown that genetic variation at *Cct6a* regulates other members of the CCT-complex in genetically
322 diverse mice[13,14]. There is no complex-wide age effect on abundance (p = 0.87) and none of the proteins
323 differ significantly in mean abundance between the two age groups (Figure 6B). In older mouse
324 cerebellum, members of the CCT-complex are correlated with more non-CCT-complex members (1,364
325 genes with r > 0.75 in older mice and r < 0.25 in younger mice), which enrich for many GO categories
326 related to its function in folding cytoskeleton proteins[38], such as the microtubule category (GO:0005874)
327 (Figures 6F & S10).

328 **CRLS is more cohesive in young female liver tissue**

329 The CRLS was found to be significantly more cohesive in livers of younger mice (p = 4.8e-57) and females
330 (p = 2.7e-8) (Figure 7A,C). There was no complex-wide age effect on abundance (p = 0.86) or any
331 significant age differences detected for individuals CRLS proteins (FDR < 0.1), whereas female liver had

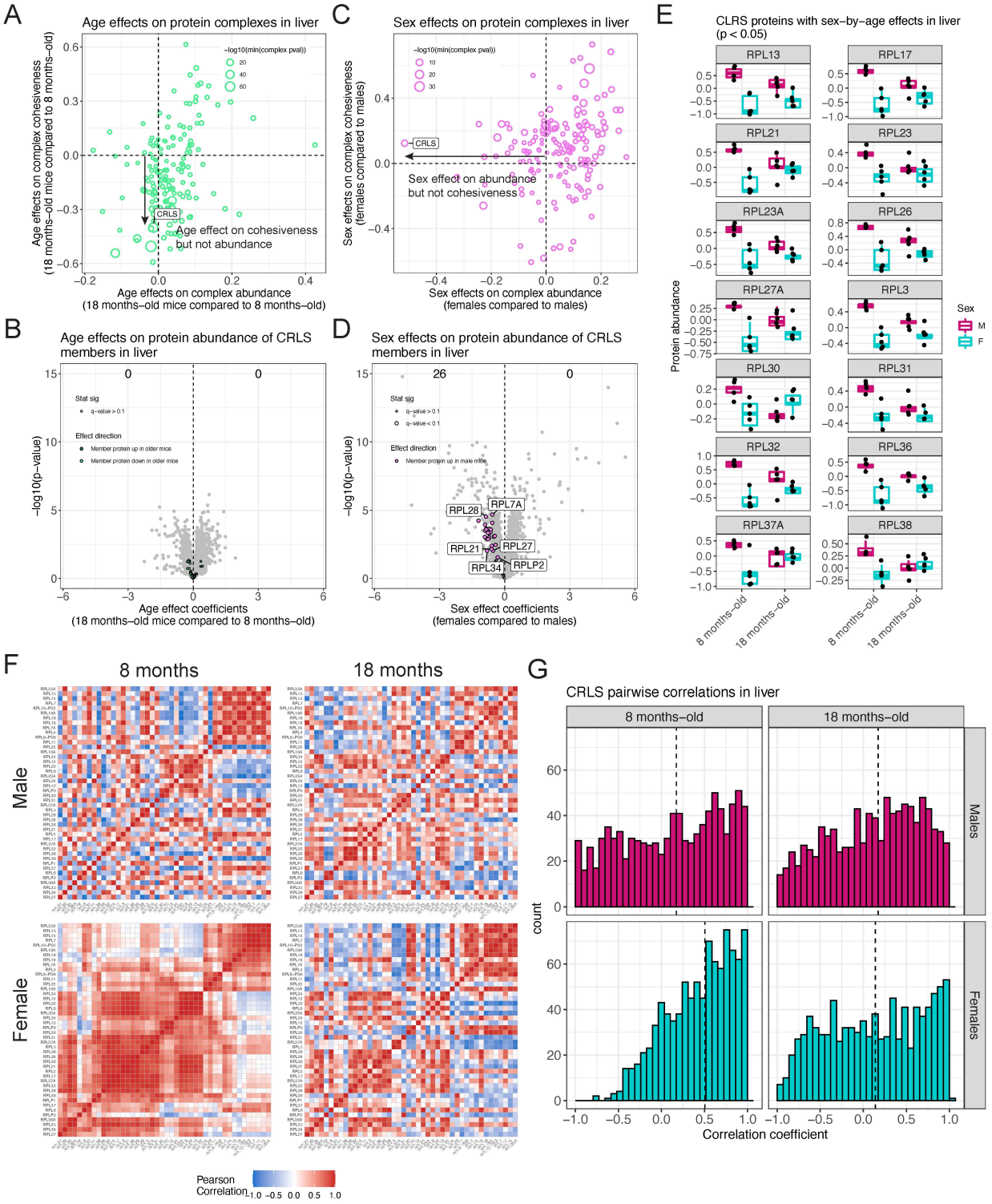

Figure 7. CRLS in liver shows sex-by-age differences in complex-wide abundance and stoichiometry. (A) Comparison of age-related differences in complex-wide correlation (y-axis) to complex-wide abundance (x-axis) in liver. Point size corresponds to the minimum p-value from the complex-wide correlation and complex-wide abundance tests on the -log10 scale. CRLS is highlighted.

(B) Volcano plot for age differences in individual protein abundance for liver with CRLS members highlighted with color based on direction of effect. Counts of proteins with significantly higher abundance in older mice and younger mice are included (FDR < 0.1).
(C) Comparison of sex-related differences in complex-wide correlation (y-axis) to complex-wide abundance (x-axis) in liver. Point size corresponds to the minimum p-value from the complex-wide correlation and complex-wide abundance tests on the -log10 scale. CRLS is highlighted.
(D) Volcano plot for sex differences in individual protein abundance for liver with CRLS members highlighted with color based on direction of effect. Counts of proteins with significantly higher abundance in females and males are included (FDR < 0.1).
(E) CRLS proteins with sex-by-age differences in abundance in liver (sex-by-age *p*-value < 0.05).
(F) Pearson correlations from the CRLS, stratified by age (younger – left and older – right) and sex (male – top and female – bottom) in mouse liver.
(F) Histograms of pairwise correlation coefficients from the CRLS, stratified by age (younger – left and older – right) and sex (male – top and female – bottom) in mouse liver. Vertical dashed lines represent median correlations.

lower complex-wide abundance (p = 2.9e-6) and significantly lower abundance for 19 proteins (Figure 7B,D). This replicates our previous finding of decreased ribosomal protein abundance in female liver tissue from genetically diverse mouse populations[14,15]. The co-occurrence of effects on individual protein abundance and complex-wide abundance and cohesiveness led us to examine the sex-by-age interaction effects on individual proteins, where 14 had sex-by-age differences (sex-by-age $p < 0.05$) with a consistent pattern of females having distinctly lower abundance in the younger mouse liver (Figure 7E). These differences contribute to the unique sex-by-age co-abundance patterns of the CRLS in the liver, which is more cohesive in young females compared to older females or males (Figures 7F-G). Notably, age and sex effects on the CRLS vary across the tissues; in lung there is a complex-wide greater abundance in older mice and little clear effect from sex (Figure S11).

DISCUSSION

We performed quantitative protein profiling across 10 tissues from the mouse reference strain, C57BL/6J. We tested for and characterized differences in protein abundance based on age, sex, and their interaction. Looking within and across tissues, we identify unique functional patterns of proteins that vary with age. Furthermore, we examine how protein complexes differ based on age and sex in terms of complex-wide abundance and cohesiveness or correlation. Collectively, these findings provide a

369 key protein perspective on aging-related changes that are globally seen across tissues as well as unique
370 to specific tissues.

371 The primary aging pattern shared across all tissues is an increase in immunoglobulin proteins,
372 implicating the immune system in the aging process. This is parallel to aging signatures in
373 transcriptomics[2], which also matched the protein data based on the strongest signal occurring in fat
374 tissues. Even in tissues like striatum and hippocampus that had very few proteins with significant age
375 differences, specific immune proteins increased in abundance with age consistent with the other tissues.
376 Given that the data represent bulk tissue samples, age effects within a tissue may be driven by changes
377 in cellular composition with age. These patterns suggest that with age changes in the adaptive immune
378 response occur, potentially due to increased presence of immunoglobulin-producing immune cell, to
379 varying degrees across tissues. This is further supported by matching increases in the
380 immunoproteasomes.

381 Additionally, we observed immune-related aging patterns that were specific to tissues, which
382 further highlights changes to the immune system as a signature of aging. In the spleen, which is has a
383 unique role in the immune system compared to the other tissues in this study, we saw reduced
384 abundance with age for proteins involved in leukocyte activation, particularly T cells. We note that many
385 of these proteins were primarily quantified in spleen. Fat also exhibited unique increases with age for
386 immune-related proteins. Together these findings point to dynamic immune system changes across
387 tissues.

388 Previous studies have demonstrated that protein complexes can be co-regulated by biological
389 factors, such as sex, diet, and genetics[13–15]. We assessed how age and sex affect complex-wide
390 abundance and cohesiveness, replicating our previous finding of reduced ribosomal protein abundance
391 in female liver[14]. We note an excess of age differences across tissues for protein complexes, both in

392 terms of cohesiveness and abundance, related to proteostasis, which is hypothesized to contribute to
393 aging[39–42], including ribosomes, proteasome, and the CCT-complex. We note that the direction of change
394 was not necessarily consistent across tissues for a complex, nor is it possible to distinguish loss of
395 stoichiometric balance with age from changes in tissue compositions, as is likely the case for the
396 immunoproteasome. Nevertheless, our findings do suggest changes to and potential disruption of
397 proteostasis with age that vary across tissues.

398 This study represents a unique quantitative protein resource for the aging-focused research
399 community. We provide our data and corresponding processed results as an interactive RShiny
400 application, available online at http://aging-b6-proteomics.jax.org, allowing proteins of interest to be
401 easily queried. This tool can be used to confirm or replicate findings from previous studies (BCAT1) or
402 other models (REN1 in aging rat kidney) and generate hypotheses for future studies of aging.
403

404 **METHODS**

405 **Data and code availability**

406 All statistical analyses were performed using the R statistical programming language (v4.0.3)[43]. All
407 starting data, key forms of processed data, and the analysis pipeline to process the data, run analysis,
408 and produce the reported findings have been made publicly available (10.6084/m9.figshare.19765849).

409 The processed data are also interactively viewable through an RShiny application, which is available
410 online (http://aging-b6-proteomics.jax.org) or can be run locally through RStudio
411 (https://github.com/gkeele/Aging_B6_Proteomics_RShiny).

412 **Mice**

413 Female and male C57BL/6J mice (stock JR#000664) were obtained from The Jackson Laboratory. Animals
414 were maintained on pine shavings and given a standard rodent diet (LabDiet 5KOG) and acidified water

415 in a pathogen free room. The room was maintained at 21°C with a 12-hour light/dark cycle (6am to
416 6pm). At the time of tissue collection (at 8 and 18 months of age) animals were euthanized by cervical
417 dislocation. All animal experiments were performed in accordance with the National Institutes of Health
418 Guide for the Care and Use of Laboratory Animals (National Research Council) and were approved by
419 The Jackson Laboratory's Animal Care and Use Committee.

420 **Sample preparation for proteomics analysis**

421 Tissue samples were dounce homogenized and resuspended in lysis buffer (8M urea, 150 mM NaCl,
422 Roche protease inhibitor tablets) and cells were lysed by sonication (procedure). Lysates were cleared
423 by centrifugation (15 min at 20,000xg) and protein concentrations were measured using Pierce BCA
424 assay kits. Proteins were then reduced with dithiothreitol (5mM for 30 minutes at room temperature)
425 and alkylated with iodoacetamide (15mM for 60 minutes in the dark). The alkylation reaction was
426 quenched by adding an additional aliquot of DTT. For each sample, 100ug of protein was aliquoted and
427 diluted to a final concentration of 1mg/mL. Proteins were digested using LysC (Wako, overnight, room
428 temperature, moderate agitation) followed by trypsin (6 hr, 37C, 200rpm). The resulting peptides were
429 then labeled with individual TMT (Thermo) reporters (1.5 hours at room temperature) and the reaction
430 was quenched with hydroxylamine (5% in water for 5 minutes). Labeled peptides were mixed into a set
431 of two plexed for each tissue analysis. After labeling and mixing, peptide mixtures were desalted using
432 C18 seppak cartridges (1mg, Waters). Desalted peptides were then fractionated using basic-pH reverse
433 phase chromatography[44]. Fractionated peptides were desalted using Stage-tips[44] prior to LC-MS/MS
434 analysis.

435 **Mass spectra data analysis**

436 Peptides were separated prior to MS/MS analysis using an Easy-nLC (Thermo) equipped with an in-
437 house pulled fused silica capillary column with integrated emitter packed with Accucore C18 media

438 (Thermo). Separation was carried out across 90-minute gradients running from 96% Buffer A (BUFFER)
439 to 30% Buffer B (BUFFER). Mass spectrometric analysis was carried out on a modified Orbitrap Fusion
440 Lumos (Thermo). Multiplexed analysis of samples was done using real-time search data acquisition[10],
441 based on canonical SPS-MS3 acquisition. Briefly, a survey MS1 scan was used to identify potential
442 peptide precursors (R = 120000, Mass range: 400-2000 m/z, max Inject time: 50ms, AGC: 200000, RF
443 lens: 30%). The top 10 precursors were selected for fragmentation and analysis in the ion trap (Dynamic
444 exclusion: 120s at 10ppm, CID collision energy: 35%, max inject time: 120ms, AGC: 20000, scan rate:
445 rapid, isolation width: 0.5 m/z). Real-time spectral matching was carried out using the Comet search
446 algorithm[45]. If, and only if, a peptide was matched with high confidence, the instrument would then
447 acquire an additional SPS-MS3 scan for quantification of relative abundances (R = 50000, HCD NCE: 65,
448 max inject time: 200ms).

449 Raw spectral information was converted to mzXML format, and spectra were matched using the Comet
450 search algorithm comparing against the ENSEMBL_GRCm39 database[45,46]. Peptides and proteins were
451 filtered to a 1% using rules of protein parsimony[45].

452 **Protein abundance estimation from peptides**

453 The abundance level for a protein was estimated as a scaled sum of its component peptides. For protein
454 j from tissue k of mouse i, the abundance is calculated as $y_{ijk} = \frac{\sum_M y'_{imk} 1_{imk}}{\theta_{ik}}$ where M is the set of
455 peptides that map to protein j, y'_{im} is the intensity of peptide m from tissue k of mouse i, 1_{imk} is the
456 indicator function that peptide m was observed in tissue k of mouse i, and $\theta_{ik} = \frac{\sum_P y'_{ip}}{\max_{l \in B[ik]} (\sum_P y'_l)}$ is the
457 within-batch scaling factor[47] for mouse i in tissue k, representing the ratio of the sum of all peptide
458 intensities for mouse i to the maximum sum total for the 11 samples in the batch of mouse i for tissue
459 k, $B[ik]$. To standardize quantities across batches, abundances were ratio normalized to a pooled

460 sample that was included in all batches: $\tilde{y}_{ijk} = \log_2\left(\frac{y_{ijk}+1}{y_{b[ik]jk}+1}\right)$ where $b[ik]$ is the bridge sample from

461 the batch of mouse i for tissue k.

462 **Filtering out low quality proteins and samples**

463 We filtered out proteins that were only observed in one of the two batches for a tissue because we

464 found single batch proteins could be influential in downstream analysis. After protein abundance

465 estimation and removal of single batch proteins, we performed PCA[48] to identify tissue samples that

466 were clear outliers across many proteins. We removed one sample from liver (young male), fat (young

467 male), spleen (old male), lung (young male), and skeletal muscle (old female). Two samples were

468 removed from striatum, both old female mice.

469 **Testing for age, sex, and sex-by-age interaction effects on proteins within tissues**

470 We tested for significant differences based on age, sex, and sex-by-age using ordinary least squares

471 (OLS) regression. For each protein j observed in tissue k, we fit the following model:

472

473 $$\tilde{y}_i = \mu + \beta_{\text{old}} x_i^{\text{old}} + \beta_{\text{female}} x_i^{\text{female}} + \beta_{\text{batch}} x_i^{\text{batch}} + \varepsilon_i$$

474 *Equation 1*

475 where μ is the intercept, β_{old} represents the effect of being in the old group, β_{female} represents the

476 effect of being female, β_{batch} represents the effect of being in second batch, x_i^{old}, x_i^{female}, and x_i^{batch} are

477 indicator variables that mouse i is old, female, or in batch2, respectively, and ε_i is the error for mouse i,

478 modeled as $\varepsilon_i \sim N(0, \sigma^2)$ and σ^2 is the variance of the noise. To test for an age effect, we used analysis

479 of variance (ANOVA), comparing the model in Equation 1 to a model excluding the age term and

480 recorded the age effect coefficients, standard errors, and *p*-values. Similarly, we tested for a sex effect

481 by comparing the Equation 1 model to a model excluding the sex term and again recorded sex effect

482 coefficients, standard errors, and *p*-values. Finally, we assessed sex-by-age effects by adding a sex-by-

483 age interaction term to the model which was then compared to the Equation 1 model with ANOVA and
484 recorded the sex-by-age *p*-value. We estimated the FDR using the Benjamini-Hochberg (BH) method[49]
485 for each effect type, producing age, sex, and sex-by-age *q*-values. This process was used each of the 10
486 tissues.

487 When plotting data (not effect parameters), we first regressed out the effect of batch to make the signal
488 from age or sex clearer. We fit the model in Equation 1 and then calculated $\tilde{\tilde{y}}_i = \tilde{y}_i - \hat{\beta}_{\text{batch}} x_i^{\text{batch}}$,
489 where $\hat{\beta}_{\text{batch}}$ is the estimated coefficient for the second batch, for all proteins j across all tissues k.

490 **Testing for consistent and unique age and sex effects on proteins across tissues**

491 We tested whether age and sex effects on a protein were similar or distinct across tissues for all proteins
492 detected in more than one tissue using linear mixed effects models (LMM) fit in the lme4 R package[50].
493 For each protein j, we fit the following model:
494

495 $$\tilde{y}_{ik} = \mu + \beta_{\text{old}} x_i^{\text{old}} + \beta_{\text{female}} x_i^{\text{female}} + \text{tissue}[k] + u_i + \varepsilon_{ik}$$

496 *Equation 2*

497 where tissue$[k]$ represents the effect of tissue k, u_i is a random term specific to mouse i, modeled as
498 $u_i \sim N(0, \tau^2)$, τ^2 is the variance component underlying the mouse-specific effect, and all other terms as
499 previously defined. A batch effect was not included because tissue and batch are highly confounded
500 (batch pairs specific to each tissue), and we are not interested in the marginal effect of either tissue or
501 batch. We tested for a consistent age effect across tissues by comparing the model in Equation 2 to
502 reduced model excluding the age effect with ANOVA using Satterthwaite's approximation for an
503 LMM[51,52], implemented in the lmerTest R package[53]. We next looked for age effects that were unique to
504 tissues or were even flipped by testing an age-by-tissue term by comparing the model in Equation 2 to
505 an expanded model that included the interaction term. The same approach was used to test for

506 consistent sex effects across tissues and tissue-unique and flipped sex effects. To account for multiple
507 testing across proteins, we again estimated q-values using the BH method[49].

508 **Modeling how factors contribute to variation in proteins measured in all 10 tissues**

509 To evaluate how various technical and biological factors contribute to variation in the abundance of
510 individual proteins, we fit an LMM with variance components for each factor for all proteins measured
511 in all 10 tissues. For each protein j, we fit the following model:

512

513 $$\tilde{y}_{ik} = \mu + \beta_{\text{old}} x_i^{\text{old}} + \beta_{\text{female}} x_i^{\text{female}} + u_i^{\text{Mouse}} + u_{t[i]}^{\text{Tag}} + u_{b[i]}^{\text{Batch}} + \varepsilon_{ik}$$

514 *Equation 3*

515 where u_i^{Mouse} is a random term specific to mouse i (20 levels), $u_{t[i]}^{\text{Tag}}$ is a random term for TMT tag t of
516 mouse i (10 levels), $u_{b[i]}^{\text{Batch}}$ is a random term for TMT batch b of mouse i (20 levels), and all other terms
517 as previously defined. Each random effect is modeled as $u_{[i]}^{\text{factor}} \sim N(0, \tau_{\text{factor}}^2)$. Proportion of variation
518 explained by each factor was calculated as $\text{VarP}_{\text{factor}} = \frac{\hat{\tau}_{\text{factor}}^2}{\hat{\tau}_{\text{Mouse}}^2 + \hat{\tau}_{\text{Tag}}^2 + \hat{\tau}_{\text{Batch}}^2 + \hat{\sigma}^2}$. For point and interval
519 estimates of the random terms, best linear unbiased predictors (BLUPs) and 95% predictive intervals
520 were used.

521 **Testing for age and sex effects on transcripts within tissues**

522 We obtained transcriptomics data reported in Schaum *et al* 2020[2], which represent 17 tissues and 10
523 age groups (1 to 27 months) from the closely related C57BL/6JN (B6N) mice. Each age group consisted of
524 samples from four males and two females, except for 24 and 27 months, which only had the four males.
525 We filtered the data to the 9 and 18 months-old age groups, which most closely match our age groups of
526 8 and 18 months. We then tested for and characterized age and sex effects (log fold change) on gene
527 expression within each tissue. We used the DESeq2 R package[54] to fit models similar to Equation 1

528 (excluding the batch covariate), but now using a negative binomial generalized linear model (GLM) to
529 accommodate that the data are gene counts. Age and sex effects on proteins and transcripts were
530 compared based on aligning Ensembl gene IDs. When plotting the data to illustrate effects, we first used
531 DESeq2's variance stabilizing transformation[55] across samples from all tissues and age groups.

532 **Summarizing protein complex co-abundance**

533 We quantified how co-abundant, *i.e.*, cohesive, a protein was with its complex[35] as the median Pearson
534 correlation coefficient between it and other complex members. An overall summary for the complex
535 was then taken as the median across all the individual medians, an approach we used previously[14]. We
536 calculated cohesiveness only for protein complexes with more than three member proteins observed for
537 a given tissue.

538 **Testing for consistent age and sex effects on abundance across a protein complex**

539 We tested for consistent age and sex effects on protein complexes with more than three observed
540 members by jointly modeling all proteins. For each protein complex c observed in tissue k, we fit the
541 following LMM for proteins $j \in J_c$:

542

543 $$\tilde{y}_{ij} = \mu + \beta_{\text{old}} x_i^{\text{old}} + \beta_{\text{female}} x_i^{\text{female}} + u_i^{\text{Mouse}} + u_j^{\text{Protein}} + \varepsilon_{ij}$$

544 *Equation 4*

545 where J_c is the set of proteins in complex c, u_j^{Protein} is a random term for protein j, modeled as
546 $u_j^{\text{Protein}} \sim N\left(0, \tau_{\text{Protein}}^2\right)$, τ_{Protein}^2 is the variance component underlying proteins, and all other terms as
547 previously defined. We tested for an age or sex effect by comparing the model in Equation 4 to either a
548 model excluding the age or sex term, respectively, through ANOVA, again with Satterthwaite's
549 approximation[51,52], producing a *p*-value. FDR was again estimated using the BH method[49] across protein
550 complexes and tissues, for age and sex separately.

551 **Testing for age and sex effect on protein complex cohesiveness**

552 Age or sex could affect how tightly co-abundant a protein complex is. We evaluated whether age or sex
553 had a consistent effect on the correlation structure of the complex using a paired *t*-test. For example,
554 with age, we calculated all the pairwise correlations between members for both age groups for a given
555 complex within a tissue: $(\boldsymbol{r}_{\text{Old}}, \boldsymbol{r}_{\text{Young}})$, resulting in a *t*-test *p*-value and effect. This process was repeated
556 based on sex. The BH method[49] was again used to estimate FDR and produce *t*-test *q*-values for both age
557 and sex. We used a more stringent significance threshold of FDR < 0.01 because correlation coefficients
558 are non-standard quantities to model with a *t*-test.

559 **Testing changes in correlation between pairs of proteins with permutations**

560 To test whether individual pairwise correlations between protein complex members differed based on
561 age or sex, we used permutations. When testing for an age difference, we swapped mouse identifiers
562 among males and among females, thus maintaining the effect of sex and potentially avoiding anti-
563 conservative permutation *p*-values. When testing for a sex difference, we swapped labels while
564 maintaining the age groups. We estimated empirical *p*-values as $\frac{1}{P}\sum_P I\left(|r_{mn}| > |r_{mn}^{(p)}|\right)$ where P is the
565 number of permutations, $I(.)$ is an indicator function, $|r_{mn}|$ is the observed absolute Pearson
566 correlation coefficient between proteins m and n, and $|r_{mn}^{(p)}|$ is the absolute Pearson correlation
567 coefficient for permutation p. We set P to 100,000.

568 **Gene set enrichment analyses**

569 We used both set-based and score-based gene set enrichment analyses and confirmed that they often
570 conferred with each other. We used the clusterProfiler R package[12] for set-based analysis, in which we
571 defined gene sets based on various criteria, such as all genes from a given tissue that have significant
572 age or sex effects on protein abundance compared to all genes analyzed in the tissue. We also evaluated
573 tissue-specific gene sets defined by the direction of the significant age or sex effect for given tissues or

574 based on how genes clustered according to age effects across the tissues. For the score-based analysis,
575 we used the fgsea R package[56] paired with GO pathways from the msigdbr R package[57]. For each tissue,
576 we input all analyzed genes with scores as the age or sex coefficients from Equation 1, standardized by
577 their standard errors. We compared GO findings between pairs of tissues by intersecting tissue-specific
578 results based on pathway ID and gene ID.
579

580 **ACKNOWLEDGEMENTS**

581 We gratefully acknowledge Vivek M. Philip and the Computational Sciences Service at The Jackson
582 Laboratory for assistance in the development of the interactive RShiny tool for querying the data. This
583 work was supported by grant funding from the National Institutes of Health (NIH): F32GM134599
584 (G.R.K.), R01GM067945 (S.P.G.), and P30AG038070 from The Jackson Laboratory Nathan Shock Center
585 of Excellence in the Basic Biology of Aging (R.K. and G.A.C.).
586

587 **AUTHOR CONTRIBUTIONS**

588 R.K., S.P.G., G.A.C., and D.K.S. conceptualized the project and designed the experiment. J.S. and D.K.S.
589 performed the experiments. G.R.K and G.A.C. designed the methodology. G.R.K. performed the analysis.
590 G.R.K. and J.Z. built the interactive webtool. G.R.K., R.K., G.A.C., and D.K.S. wrote the manuscript. All
591 authors reviewed the manuscript.
592

593 **REFERENCES**

594 1. López-Otín, C., Blasco, M. A., Partridge, L., Serrano, M. & Kroemer, G. The Hallmarks of Aging. *Cell*
595 **153**, 1194–1217 (2013).
596 2. Schaum, N. *et al.* Ageing hallmarks exhibit organ-specific temporal signatures. *Nature* **583**, 596–602
597 (2020).

598 3. The Tabula Muris Consortium *et al.* A single-cell transcriptomic atlas characterizes ageing tissues in
599 the mouse. *Nature* **583**, 590–595 (2020).
600 4. Shokhirev, M. N. & Johnson, A. A. Modeling the human aging transcriptome across tissues, health
601 status, and sex. *Aging Cell* **20**, (2021).
602 5. Zeng, L. *et al.* Transcriptome analysis reveals the difference between "healthy" and "common" aging
603 and their connection with age-related diseases. *Aging Cell* **19**, (2020).
604 6. Takemon, Y. *et al.* Proteomic and transcriptomic profiling reveal different aspects of aging in the
605 kidney. *eLife* **10**, e62585 (2021).
606 7. Gerdes Gyuricza, I. *et al.* Genome-wide transcript and protein analysis highlights the role of protein
607 homeostasis in the aging mouse heart. *Genome Res* gr.275672.121 (2022)
608 doi:10.1101/gr.275672.121.
609 8. Kelmer Sacramento, E. *et al.* Reduced proteasome activity in the aging brain results in ribosome
610 stoichiometry loss and aggregation. *Mol Syst Biol* **16**, (2020).
611 9. Anisimova, A. S. *et al.* Multifaceted deregulation of gene expression and protein synthesis with age.
612 *Proc Natl Acad Sci USA* **117**, 15581–15590 (2020).
613 10. Schweppe, D. K. *et al.* Full-Featured, Real-Time Database Searching Platform Enables Fast and
614 Accurate Multiplexed Quantitative Proteomics. *J. Proteome Res.* **19**, 2026–2034 (2020).
615 11. Conway, J. R., Lex, A. & Gehlenborg, N. UpSetR: an R package for the visualization of intersecting
616 sets and their properties. *Bioinformatics* **33**, 2938–2940 (2017).
617 12. Yu, G., Wang, L.-G., Han, Y. & He, Q.-Y. clusterProfiler: an R Package for Comparing Biological
618 Themes Among Gene Clusters. *OMICS: A Journal of Integrative Biology* **16**, 284–287 (2012).
619 13. Chick, J. M. *et al.* Defining the consequences of genetic variation on a proteome-wide scale.
620 *Nature* **534**, 500–505 (2016).

621 14. Keele, G. R. *et al.* Regulation of protein abundance in genetically diverse mouse populations. *Cell*
622 *Genomics* 100003 (2021) doi:10.1016/j.xgen.2021.100003.
623 15. Romanov, N. *et al.* Disentangling Genetic and Environmental Effects on the Proteotypes of
624 Individuals. *Cell* **177**, 1308-1318.e10 (2019).
625 16. Williams, E. G. *et al. Multi-Omic Profiling of the Liver Across Diets and Age in a Diverse Mouse*
626 *Population*. http://biorxiv.org/lookup/doi/10.1101/2020.08.20.222968 (2020)
627 doi:10.1101/2020.08.20.222968.
628 17. Zhang, L. & Han, J. Branched-chain amino acid transaminase 1 (BCAT1) promotes the growth of
629 breast cancer cells through improving mTOR-mediated mitochondrial biogenesis and function.
630 *Biochemical and Biophysical Research Communications* **486**, 224–231 (2017).
631 18. Jung, F., Kennefick, M., Ingelfinger, R. & Vora, P. Down-Peg ulation of the Intra renal Pen In-Ang
632 iotensi n System in the Aging Pat1'2. *Journal of the American Society of Nephrology* 8.
633 19. Timmers, P. R. H. J. *et al.* Mendelian randomization of genetically independent aging phenotypes
634 identifies LPA and VCAM1 as biological targets for human aging. *Nat Aging* **2**, 19–30 (2022).
635 20. Yousef, H. *et al.* Aged blood impairs hippocampal neural precursor activity and activates
636 microglia via brain endothelial cell VCAM1. *Nat Med* **25**, 988–1000 (2019).
637 21. Perner, C. *et al.* Plasma VCAM1 levels correlate with disease severity in Parkinson's disease. *J*
638 *Neuroinflammation* **16**, 94 (2019).
639 22. Marshall, R. S. & Vierstra, R. D. Dynamic Regulation of the 26S Proteasome: From Synthesis to
640 Degradation. *Front Mol Biosci* **6**, 40 (2019).
641 23. Murata, S., Takahama, Y., Kasahara, M. & Tanaka, K. The immunoproteasome and
642 thymoproteasome: functions, evolution and human disease. *Nat Immunol* **19**, 923–931 (2018).

643 24. Kimura, H., Caturegli, P., Takahashi, M. & Suzuki, K. New Insights into the Function of the
644 Immunoproteasome in Immune and Nonimmune Cells. *Journal of Immunology Research* **2015**,
645 e541984 (2015).
646 25. Phillips, B. P., Gomez-Navarro, N. & Miller, E. A. Protein quality control in the endoplasmic
647 reticulum. *Current Opinion in Cell Biology* **65**, 96–102 (2020).
648 26. Guna, A., Volkmar, N., Christianson, J. C. & Hegde, R. S. The ER membrane protein complex is a
649 transmembrane domain insertase. *Science* **359**, 470–473 (2018).
650 27. Shurtleff, M. J. *et al.* The ER membrane protein complex interacts cotranslationally to enable
651 biogenesis of multipass membrane proteins. *eLife* **7**, e37018 (2018).
652 28. Szul, T. & Sztul, E. COPII and COPI Traffic at the ER-Golgi Interface. *Physiology* **26**, 348–364
653 (2011).
654 29. Huttlin, E. L. *et al.* Dual proteome-scale networks reveal cell-specific remodeling of the human
655 interactome. *Cell* **184**, 3022-3040.e28 (2021).
656 30. Huttlin, E. L. *et al.* The BioPlex Network: A Systematic Exploration of the Human Interactome.
657 *Cell* **162**, 425–440 (2015).
658 31. Szklarczyk, D. *et al.* STRING v11: protein–protein association networks with increased coverage,
659 supporting functional discovery in genome-wide experimental datasets. *Nucleic Acids Research* **47**,
660 D607–D613 (2019).
661 32. Lapek, J. D. *et al.* Detection of dysregulated protein-association networks by high-throughput
662 proteomics predicts cancer vulnerabilities. *Nat Biotechnol* **35**, 983–989 (2017).
663 33. Taggart, J. C., Zauber, H., Selbach, M., Li, G.-W. & McShane, E. Keeping the Proportions of
664 Protein Complex Components in Check. *Cell Systems* **10**, 125–132 (2020).
665 34. Giurgiu, M. *et al.* CORUM: the comprehensive resource of mammalian protein complexes—
666 2019. *Nucleic Acids Research* **47**, D559–D563 (2019).

667 35. Ori, A. *et al.* Spatiotemporal variation of mammalian protein complex stoichiometries. *Genome*
668 *Biol* **17**, 47 (2016).
669 36. Leitner, A. *et al.* The Molecular Architecture of the Eukaryotic Chaperonin TRiC/CCT. *Structure*
670 **20**, 814–825 (2012).
671 37. Kalisman, N., Adams, C. M. & Levitt, M. Subunit order of eukaryotic TRiC/CCT chaperonin by
672 cross-linking, mass spectrometry, and combinatorial homology modeling. *Proceedings of the National*
673 *Academy of Sciences* **109**, 2884–2889 (2012).
674 38. Grantham, J. The Molecular Chaperone CCT/TRiC: An Essential Component of Proteostasis and a
675 Potential Modulator of Protein Aggregation. *Front. Genet.* **11**, 172 (2020).
676 39. Toyama, B. H. & Hetzer, M. W. Protein homeostasis: live long, won't prosper. *Nat Rev Mol Cell*
677 *Biol* **14**, 55–61 (2013).
678 40. Cheng, J. *et al.* The emerging roles of protein homeostasis-governing pathways in Alzheimer's
679 disease. *Aging Cell* **17**, e12801 (2018).
680 41. Morimoto, R. I. & Cuervo, A. M. Proteostasis and the Aging Proteome in Health and Disease. *The*
681 *Journals of Gerontology Series A: Biological Sciences and Medical Sciences* **69**, S33–S38 (2014).
682 42. Morimoto, R. I. & Cuervo, A. M. Protein Homeostasis and Aging: Taking Care of Proteins From
683 the Cradle to the Grave. *The Journals of Gerontology Series A: Biological Sciences and Medical*
684 *Sciences* **64A**, 167–170 (2009).
685 43. R Core Team. *R: A Language and Environment for Statistical Computing*. (R Foundation for
686 Statistical Computing, 2020).
687 44. Navarrete-Perea, J., Yu, Q., Gygi, S. P. & Paulo, J. A. Streamlined Tandem Mass Tag (SL-TMT)
688 Protocol: An Efficient Strategy for Quantitative (Phospho)proteome Profiling Using Tandem Mass Tag-
689 Synchronous Precursor Selection-MS3. *J. Proteome Res.* **17**, 2226–2236 (2018).

690 45. Eng, J. K., Jahan, T. A. & Hoopmann, M. R. Comet: An open-source MS/MS sequence database
691 search tool. *Proteomics* **13**, 22–24 (2013).
692 46. Cunningham, F. *et al.* Ensembl 2022. *Nucleic Acids Research* **50**, D988–D995 (2021).
693 47. Huttlin, E. L. *et al.* A Tissue-Specific Atlas of Mouse Protein Phosphorylation and Expression. *Cell*
694 **143**, 1174–1189 (2010).
695 48. Stacklies, W., Redestig, H., Scholz, M., Walther, D. & Selbig, J. pcaMethods—a bioconductor
696 package providing PCA methods for incomplete data. *Bioinformatics* **23**, 1164–1167 (2007).
697 49. Benjamini, Y. & Hochberg, Y. Controlling the False Discovery Rate: A Practical and Powerful
698 Approach to Multiple Testing. *Journal of the Royal Statistical Society. Series B (Methodological)* **57**,
699 289–300 (1995).
700 50. Bates, D., Mächler, M., Bolker, B. & Walker, S. Fitting Linear Mixed-Effects Models Using lme4.
701 *Journal of Statistical Software* **67**, 1–48 (2015).
702 51. Giesbrecht, F. G. & Burns, J. C. Two-Stage Analysis Based on a Mixed Model: Large-Sample
703 Asymptotic Theory and Small-Sample Simulation Results. *Biometrics* **41**, 477–486 (1985).
704 52. Hrong-Tai Fai, Alex. & Cornelius, P. L. Approximate F-tests of multiple degree of freedom
705 hypotheses in generalized least squares analyses of unbalanced split-plot experiments. *null* **54**, 363–
706 378 (1996).
707 53. Kuznetsova, A., Brockhoff, P. B. & Christensen, R. H. B. **lmerTest** Package: Tests in Linear Mixed
708 Effects Models. *J. Stat. Soft.* **82**, (2017).
709 54. Love, M. I., Huber, W. & Anders, S. Moderated estimation of fold change and dispersion for
710 RNA-seq data with DESeq2. *Genome Biol* **15**, 550 (2014).
711 55. Anders, S. & Huber, W. Differential expression analysis for sequence count data. 12 (2010).
712 56. Korotkevich, G. *et al.* Fast gene set enrichment analysis. *bioRxiv* 060012 (2021)
713 doi:10.1101/060012.

714 57. Dolgalev, I. *msigdbr: MSigDB Gene Sets for Multiple Organisms in a Tidy Data Format*. (2021).

715

716